Generation of B-Doped Graphene Nanoplatelets Using a Solution Process and Their Supercapacitor Applications

Jongwoo Han,[†,⊥] Li Li Zhang,[‡,⊥] Seungjun Lee,[†] Junghoon Oh,[†] Kyoung-Seok Lee,[§] Jeffrey R. Potts,[‡] Junyi Ji,[‡] Xin Zhao,[‡] Rodney S. Ruoff,[‡] and Sungjin Park[†,*]

[†]Department of Chemistry, Inha University, 100 Inha-ro, Nam-gu, Incheon, 402-751 Korea, [‡]Department of Mechanical Engineering and the Materials Science and Engineering Program, The University of Texas at Austin, One University Station C2200, Austin, Texas 78712-0292, United States, and [§]Center for Analytical Chemistry and Korea Research Institute of Standards and Science, Yuseong, Daejeon 305-340, Korea. [⊥]These authors equally contributed to this work.

ABSTRACT Chemically modified graphene (CMG) nanoplatelets have shown great promise in various applications due to their electrical properties and high surface area. Chemical doping is one of the most effective methods to tune the electronic properties of graphene materials. In this work, novel B-doped nanoplatelets (borane-reduced graphene oxide, B-rG-O) were produced on a large scale *via* the reduction of graphene oxide by a borane-tetrahydrofuran adduct under reflux, and their use for supercapacitor electrodes was studied. This is the first report on the production of B-doped graphene nanoplatelets from a solution process and on the use of B-doped graphene materials in supercapacitors. The B-rG-O had a high specific surface area of 466 m^2/g and showed excellent supercapacitor performance including a high specific capacitance of 200 F/g in aqueous electrolyte as well as superior surface area-normalized capacitance to typical carbon-based supercapacitor materials and good stability after 4500 cycles. Two- and three-electrode cell measurements showed that energy storage in the B-rG-O supercapacitors was contributed by ion adsorption on the surface of the nanoplatelets in addition to electrochemical redox reactions.

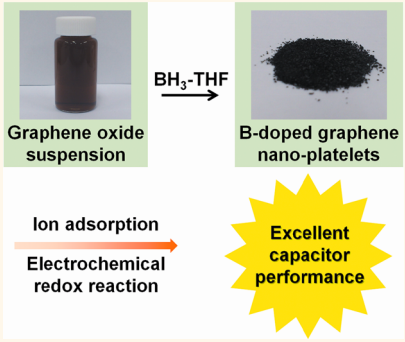

KEYWORDS: graphene · graphene oxide · boron doping · supercapacitor · solution process

Carbon materials have shown excellent performance as electrodes, catalysts, and supports for energy devices such as supercapacitors, batteries, fuel cells, photovoltaic cells, and hydrogen storage materials.[1−4] Recently, graphene, which is composed of one atom thick sp^2 carbon network, shows great potential for industrial applications due to excellent electrical properties and high surface area.[2,3,5−8] Chemical doping is one of the most effective methods to tailor the electronic properties of graphene-based conductive materials. N- or B-doped graphene-based materials have shown enhanced electrical properties relative to the materials without doping.[9−11] There are a few examples of the production of B-doped CMGs using high temperature processes with gas-phase boron sources or autoclave treatments under inert gas.[10,12,13] However, mass production of such B-doped CMGs using a solution-based process could be much more cost-effective than these methods.

Recently, the use of chemically modified graphene (CMG) nanoplatelets in supercapacitors has shown great promise for industrial applications.[3,14−21] CMG materials have several advantages for use as supercapacitor electrodes such as high accessible surface area, good electrical conductivity, feasible mass production *via* solution-based processing, and the low cost of graphite as a starting material. Supercapacitors are electrochemical energy storage devices that store and release energy by reversible adsorption and desorption of ions at the interfaces between electrode materials and electrolytes.[22] Stoller *et al.*, first demonstrated the use of CMG materials as supercapacitor electrodes.[15] Two general classes of CMG-based electrodes have been studied: (i) CMG materials with large surface areas[1,15,16,23,24] and (ii) hybrid systems composed of CMGs and pseudocapacitor materials, such as metal oxides and conducting polymers,[1,25−29] which use fast redox reactions at the large surfaces of such electrode

* Address correspondence to sungjinpark@inha.ac.kr.

Received for review July 31, 2012 and accepted December 17, 2012.

Published online December 17, 2012
10.1021/nn3034309

materials for charge storage. However, further improvements in electrode materials and understanding the relationship between electrode structure and supercapacitor performance of such materials remain a major challenge.

The surface area of electrode materials is one of the critical factors that affect specific capacitance. However, it has been found that the electronic properties of electrode materials play an important role in determining capacitor performance.[30] CMG materials doped with electron-rich N atoms show good performance as supercapacitor electrodes.[1] However, the performance of B-doped graphene-based materials in supercapacitor electrodes has not been studied to date.

B-doping in other types of carbon materials has enhanced the performance when used as supercapacitor electrodes.[6,31−34] Cheng *et al.*, reported a low-level boron-doped mesoporous carbon (BMC).[31] It was found that the BMC exhibited higher capacitance compared to the undoped mesoporous carbon, due to the presence of B, with values of 110−130 F/g over a range of current densities.

In this work, novel B-doped CMG nanoplatelets were made by reduction of graphene oxide with a borane (BH_3)-tetrahydrofuran (THF) adduct under reflux *via* a one pot synthesis using a liquid process on a large scale. Such borane-reduced graphene oxide (B-rG-O) contained small amounts of B components and showed excellent supercapacitor behavior including high specific capacitance values of 200 F/g with a good rate performance using an aqueous electrolyte.

RESULTS AND DISCUSSION

Suspensions of graphene oxide are currently the most promising precursors to production of CMG nanoplatelets on a large scale.[5,34] A brown aqueous suspension of graphene oxide was produced by sonication of graphite oxide (GO) powder that produced by oxidation of natural graphite using the modified Hummers method.[35] During the oxidation process, the sp^2 network of graphite is significantly disrupted and a wide range of oxygen functional groups is introduced, including hydroxyl and epoxy groups on the basal planes and carboxylic acid and ketone groups at the edges.[34,36,37] The resulting graphite/graphene oxides are electrically insulating.

Borane was added into the aqueous graphene oxide suspension at room temperature, and the resulting aqueous suspension was stirred under reflux. Since a B atom in BH_3 does not satisfy the octet rule, it usually exists as a gas-phase dimer, B_2H_6, or in an adduct form with a Lewis base.[38] In this work, we used a liquid borane−THF adduct (Figure 1a) because it is more easily adaptable to a liquid process compared with gas-phase reagents such as B_2H_6. Black agglomerated powders (B-rG-O) precipitated from the suspension after reflux (reaction temperature, 100 °C), which is a

Figure 1. (a) A borane−THF adduct, (b) a reaction scheme of the reduction of graphene oxide with the borane−THF adduct, (c) SEM images of B-rG-O powder at different magnifications.

typical result when carbon networks of graphene oxide are graphitized *via* removal of oxygen functionalities. A powder conductivity measurement of the B-rG-O samples yielded 50 S/m.

We found that the graphene oxide was reduced by the reaction with borane−THF under reflux. The samples used in this work were allowed to react for four days under reflux; the reaction time and temperature (100 °C) are critical parameters in this reduction system (see Supporting Information (SI)). For example, when the reaction was done on an oil bath set at 60 or 80 °C, the product (B-G-O, see SI) had a much lower degree of reduction than the B-rG-O obtained under reflux.

Figure 1c shows SEM images of dried particles of B-rG-O at different magnifications. The images show how the surfaces of the B-rG-O particles, composed of agglomerated individual layers, are exposed to the electrolyte. The surface area of B-rG-O powders determined by Brunauer−Emmett−Teller (BET) measurements using N_2 absorption was as high as 466 m^2/g with that particular sample having an average pore size of 2.13 nm. While the specific surface area is much lower than the theoretical value (2630 m^2/g) of a pristine graphene sheet, the BET value of B-rG-O nonetheless suggests its potential for use as an electrode material in supercapacitors with results from prior work.

Incorporation of B components in B-rG-O was characterized by X-ray photoelectron spectroscopy (XPS) and also by inductive coupled plasma mass spectrometry (ICP−MS) of B-rG-O powder samples (see SI for the ICP−MS analysis). While no trace of B was found in an XPS spectrum of GO powder, small amounts (1.1 atom % and 0.7 atom % from two samples respectively) of B were found near 192 eV in the spectrum of B-rG-O (Figure 2a). The small peak could be assigned to be a BC_2 component,[10,12,33,39,40] suggesting that boron was attached on the B-rG-O nanoplatelets. Residual boron compounds, such as boron oxides that are easily

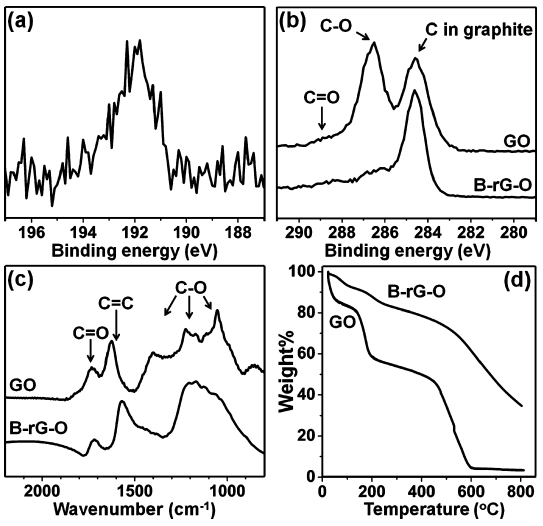

Figure 2. (a) B1*s* XPS spectrum of B-rG-O and (b) C1*s* XPS spectra, (c) FT-IR spectra, and (d) TGA curves of GO and B-rG-O.

generated by the reaction of borane and water, could have been adsorbed on the product. Thus, we prepared boron oxides by the reaction of BH_3—THF in water under reflux and an XPS spectrum of the boron oxides showed a peak around 193 eV (data not shown here). In the XPS spectrum of B-rG-O, there was no peak between 193 and 194 eV, corresponding to boron oxides.[12,40] The residual oxide forms, which may be produced in this reaction, should be completely washed out by water. The existence of free borane or B—B species was also excluded because there was no peak between 187 and 188 eV.[10,40] To further confirm no presence of boron residues, the B-rG-O powder was washed with water five more times. The XPS spectrum of this sample was almost the same as that of B-rG-O, meaning that B components were incorporated into the B-rG-O nanoplatelets. To the best of our knowledge, this is the first report for the production of B-doped CMG materials using a liquid process.

As shown in Figure 2b, an XPS spectrum of GO powders in the C1*s* region showed the existence of oxygen-containing components: a peak around 287 eV, corresponding to C—O moieties such as epoxy and hydroxyl groups on the basal planes, and a small tail around 289 eV, corresponding to C═O moieties such as carboxyl and ketone groups at the edges. A peak at 284.6 eV corresponds to graphitic carbons.[41,42] After treatment of graphene oxide with a borane—THF adduct, the peaks corresponding to C—O moieties were significantly diminished in intensity. This means that a large portion of the hydroxyl and epoxy groups on the basal planes was removed by the borane—THF treatment. The tail around 289 eV was still observed in an XPS spectrum of the B-rG-O. Although there has been no report on the reaction between borane species and graphene oxide, it is well-known that oxygen functionalities such as ketone, carboxylic acid, and hydroxyl groups can be removed by eletrophilic boranes *via* reductive deoxygenation for small organic molecules.[43—45]

We also performed combustion-based elemental analysis as the C/O ratio has been used to evaluate the degree of reduction in rG-O-type materials. While a typical C/O ratio of GO is about 1.3,[35,46] the C/O ratio of B-rG-O was about 7.8, indicating a high degree of reduction of the B-rG-O material. The Fourier transformed infrared (FT-IR) spectrum (Figure 2c) of GO showed C═C, C═O, and C—O stretches as previously assigned.[41] The intensity of the C═C stretch relative to the C═O stretch increased after borane treatment of graphene oxide. An FT-IR spectrum of GO showed C—O stretches of epoxy and hydroxyl groups between 1100 and 1200 cm^{-1}, and the spectrum of B-rG-O also showed broad peaks in this region. These modes might be contributed by a combination of single bond stretches between C, O, and B atoms.[47]

As a control experiment to study the role of borane as a potential reducing agent, an aqueous suspension of graphene oxide was stirred under reflux for 4 days without the borane—THF adduct, which yielded reduced graphene oxide ("4d-rG-O"). The C/O ratio (5.0) of 4d-rG-O obtained by elemental analysis showed that its degree of reduction was lower than that of B-rG-O (see SI for further details of the analysis of the 4d-rG-O sample). The results taken together suggest that graphene oxide was reduced by both the combination of the borane species and by the long time reflux.

As illustrated in Figure 2d, thermogravimetric analysis (TGA) curves show that B-rG-O powder was more thermally stable than GO powder. Both GO and B-rG-O showed significant weight loss before 100 °C due to evaporation of water molecules. However, the weight loss (7 wt %) of B-rG-O was much smaller than that (17 wt %) of GO in this region, suggesting that the water content in B-rG-O was much smaller than that in GO.[46,48] The second weight loss event was observed between 100 and 200 °C due to a loss of CO and CO_2 by thermal decomposition of labile oxygen functionalities and possibly, evaporation of remaining water molecules.[48] The weight loss of B-rG-O (12 wt %) in this temperature region is significantly smaller than that of GO (~40 wt %). As described above, these chemical analyses evidently show the successful reduction of graphene oxide by a borane—THF adduct and suggest that the resulting B-rG-O material, which has a high surface area and has B-doped sp^2 carbon networks, could be a good candidate for various applications such as an electrode material in supercapacitors and *p*-type doped electronic devices.

As an example of a possible application of B-rG-O nanoplatelets, the electrochemical performance of the B-rG-O nanoplatelets as supercapacitor electrode materials was studied using two-electrode and three-electrode configurations (see SI for images of

TABLE 1. Specific Capacitance of B-rG-O Electrodes (F/g)

cell configuration	0.1 A/g	0.5 A/g	1 A/g	3 A/g	5 A/g
two-electrode	200	177	160	146	140
three-electrode	193	165	155	144	

electrodes) using an aqueous KOH solution (6 M) as the electrolyte. Table 1 shows values of specific capacitance of B-rG-O electrodes in both two- and three-electrode systems at various current densities. Cyclic voltammetry (CV) testing with a two-electrode symmetrical supercapacitor cell was performed at various scan rates as shown in Figure 3a. The B-rG-O had a specific capacitance value of 200 F/g in aqueous electrolyte (Figure 3b).

The near-rectangular CV curve obtained at a high scan rate of 100 mV/s (Figure 3a) indicated a low resistance of B-rG-O electrodes to mass transfer and good charge propagation of ions at the interfaces between the electrolyte and the B-rG-O material. Compared to porous materials of high surface area, the surface area of CMG nanoplatelets does not depend on the distribution of a pore size. CMG nanoplatelets, which are compliant, and high aspect ratio platelets even when agglomerated, can physically "move" or conform to improve accessibility of their surfaces to electrolytes.[2,15] Thus, ions in the electrolyte can migrate throughout the interstices of the agglomerated CMG network to access the large internal surface area of the B-rG-O particles. The interstitial network of agglomerated CMG nanoplatelets may provide a less tortuous diffusion path for ions than conventional high surface area porous materials, resulting in the high energy storage capability as well as good power delivery of CMG-based supercapacitor electrodes.

The rate-dependent specific capacitance and surface area-normalized capacitance is shown in Figure 3b. The specific capacitance decreased slightly from 200 to 160 F/g when the current loading was increased 10-fold from 0.1 to 1 A/g, indicating an excellent rate response of the B-rG-O electrode. This behavior could be explained by the kinetics of ion diffusion in the B-rG-O electrode, which was investigated using electrochemical impedance spectroscopy. Figure 3c shows a Nyquist plot obtained over the frequency range from 1000 kHz to 0.01 Hz, with an expanded view of the high frequency region in the inset. The near-vertical slope in the plot over the low frequency region indicates good capacitor behavior of the cell. The equivalent series resistance obtained from the *x*-intercept of the Nyquist plot (Figure 3c inset) is quite small at about 0.8 Ω, suggesting that the B-rG-O electrode has a low resistance. The midhigh frequency Nyquist plot intersects the real axis at a 45° angle, which is due to the transport of ions within the electrode. A short 45° slope portion of the plot indicates fast diffusion of the electrolyte ions within the B-rG-O electrode.

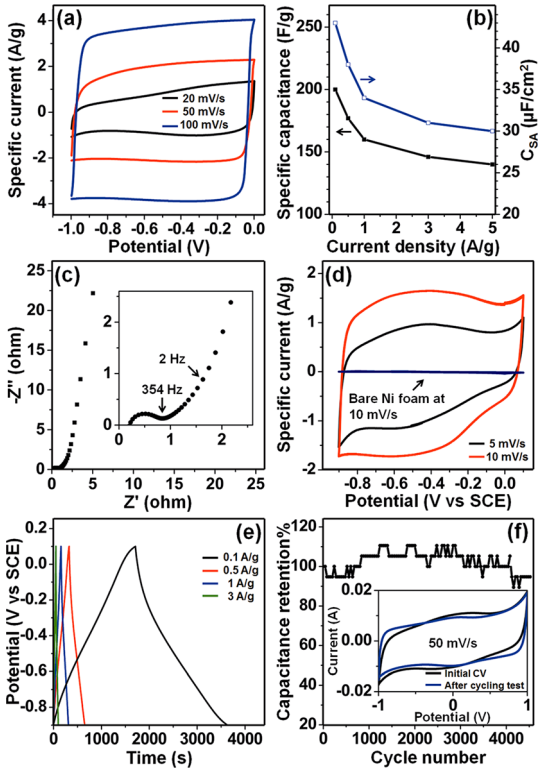

Figure 3. The electrochemical performance of a B-rG-O electrode in 6 M KOH solution using a two-electrode configuration, showing (a) CV curves at various scan rates, line segments connecting points added as a guide to the eye, (b) gravimetric capacitance and surface-area normalized capacitance at various scan rates, and (c) a Nyquist plot showing the imaginary part *versus* the real part of impedance (the inset of Figure 3c shows the high frequency region of the Nyquist plot), (d) CV curves at various scan rates using a three-electrode configuration, (e) galvanostatic charge/discharge curves under different current densities, (f) cycling performance using a two-electrode configuration (inset shows the CV curves at the scan rate of 50 mV/s before and after the cycling test, 4500 cycles).

More importantly, the BET surface area-normalized capacitance (C_{SA}, see the Methods section) is as high as 43 μF/cm^2 at a low current density of 0.1 A/g (Figure 3b), much higher than the capacitance that could be realized purely from EDL on the carbon surface, which is typically in the range of 10−30 μF/cm^2.[14,21] The C_{SA} consistently remained above 30 μF/cm^2 over the entire range of scan rates. It suggests that the B-rG-O, which contains B-doped graphene networks with some oxygen functionalities such as hydroxyl and carboxylic acid groups, could have additional mechanisms contributing to its capacitance beyond just EDL capacitance. Additionally, the CV curve at a low scan rate of 20 mV/s as shown in Figure 3a is not close to a rectangular shape. Consequently, we examined the B-rG-O systems with three-electrode cell systems to study the pseudocapacitance characteristics of the current electrode material.

Figures 3 panels d and e show the CV curves of B-rG-O with low scan rates of 5 and 10 mV/s and galvanostatic

charge–discharge plots at different current densities obtained by three-electrode cell measurement using a 6 M KOH electrolyte. A pair of anodic and cathodic wide humps was observed, with much more pronounced redox humps apparent at the lower scan rates. These humps are an indication of the presence of reversible faradic reactions that are associated with electrochemically active functionalities on the electrode surface. The rectangular-like shape along with a pair of redox humps suggested that the capacitive response comes from a combination of pseudocapacitance and EDL capacitance. Pseudocapacitance, which is the product of electrochemical redox reactions on the surface, may come from both B- and/or O-functionalities of B-rG-O.[17−19,31−33,49,50] In addition, it has been reported that electron-deficient boron doping in the other types of carbon materials increases the pseudocapacitance.[31,33]

To further understand the effect of boron doping, we tested the electrochemical performance of the 4d-rG-O sample (see above and SI for discussion of its synthesis and analysis). Various characterizations showed that the 4d-rG-O sample has similar physical and chemical properties to that of the B-rG-O sample (BET surface area of 403 *vs* 466 m^2/g, C/O ratio of 5.0 *vs* 7.8, and effective series resistance of 1 ohm *vs* 0.8 ohm for samples 4d-rG-O and B-rG-O, respectively) except for boron doping. The electrochemical performance of the 4d-rG-O sample as a supercapacitor electrode was evaluated under the same test conditions as that used for B-rG-O and the results are shown in SI, Figures S8 and S9. The CV curves of the 4d-rG-O electrode in a three-electrode configuration (Figure S8) showed wide redox humps, indicating the presence of the O-functionalities in the 4d-rG-O electrode. The redox humps are more pronounced in the 4d-rG-O electrode than in the B-rG-O electrode, implying a larger concentration of O-functionalities in the 4d-rG-O sample. Though O-functionalities are present in both 4d-rG-O and B-rG-O electrodes, the specific capacitance of 4d-rG-O is much lower than that of the B-rG-O electrode (96 *vs* 177 F/g at a current density of 0.5 A/g for 4d-rG-O and B-rG-O, respectively). In addition, the BET area-normalized capacitance for 4d-rG-O is 23 uF/cm^2, which is smaller than that of the B-rG-O electrode. Taking consideration of a similar or higher O content in the 4d-rG-O material, the significant enhancement of the specific capacitance of the B-rG-O electrode is thus likely from the B-doping effect.

It is known that the introduction of electron–donor and/or electron–acceptors into graphene can significantly change the electronic structure of few-layer graphene.[10] Our recent study has clearly demonstrated that a small amount of N-dopant in graphene changes the electronic structure and density of state (DOS) significantly, modifies the quantum capacitance, and leads to larger values for the interfacial capacitance.[51] Cheng *et al.*, also reported that low-level boron doping can improve the interfacial capacitance compared to boron-free carbon of a similar morphology and type.[31] The boron doping of graphene-based nanoplatelets as described here likely also changes the electronic structure, leading to an enhancement of capacitance of the B-rG-O.

The cycling performance of the B-rG-O electrode in 6 M KOH electrolyte (with two-electrode configuration) at a current density of 1 A/g is displayed in Figure 3f. More than 95% of the original capacity was retained after 4500 cycles, and no distortion of the CV curves was observed after the cycle test, indicating a stable electrode material under the environment used in this work. The Ragone plot (SI, Figure S10) also shows the B-rG-O electrode has good power densities and moderate energy densities.

The hybrid systems of EDL capacitance and pseudocapacitance have been studied to enhance the capacitance of electrode materials; some examples are composites composed of CMGs and metal oxides or polymers.[1,25−29] However, the performance of composite electrodes can vary significantly depending on morphological characteristics such as particle dispersion, giving this single-component CMG platelet system an advantage for reproducibility. Overall, the B-rG-O nanoplatelets possess a significantly improved capacitance compared with other CMG materials, and also exhibit good rate and stability performance.

In this work, we used a new reducing agent, borane, for graphene oxide. In a separate control experiment where only THF instead of a borane–THF adduct is present in the system, there was no reduction of graphene oxide (data not shown here). Although sodium borohydride ($NaBH_4$), which contains a boron atom, has been reported as an effective reducing agent for graphene oxide,[52,53] B-doping in graphene-based materials reduced using $NaBH_4$ has not been reported. It has been thought that a nucleophile-type hydride form, BH_4^-, acts as a reducing chemical species for graphene oxide with the use of $NaBH_4$. When borane–THF adducts are dissolved in water, the borane usually dissociates from the THF.[38] Since isolated borane is not satisfied by the octet rule, it is a highly electrophilic species. Consequently, electron-rich oxygen groups of the graphene oxide might be removed from the graphene oxide by the borane *via* reductive deoxygenation.[34,36,37] This reduction could be an electrophile-assisted reduction of graphene oxide, which is unique given that most common reducing agents for graphene oxide are nucleophilic.

CONCLUSION

We synthesized B-doped CMG nanoplatelets (B-rG-O) using a liquid process, *via* the reaction of an aqueous colloidal suspension of graphene oxide with a borane–THF adduct under reflux. During the reaction, the graphene oxide was reduced by the treatment of the borane adduct and a small amount of B atoms were

incorporated into the CMG nanoplatelets, as confirmed by XPS, TGA, FT-IR, ICP–MS, and elemental analysis. This example could open new routes to produce B-doped graphene nanoplatelets using a liquid-phase process. Additionally, the B-doped graphene nanoplatelets could be useful for applications such as sensors, polymer composites, and electric devices.

The B-rG-O nanoplatelets had a high specific surface area of 466 m^2/g and were tested as an electrode material in supercapacitors with two-electrode and three-electrode configurations. B-rG-O showed excellent performance as a supercapacitor electrode material in aqueous electrolyte (6 M KOH). The specific capacitance of B-rG-O was as high as 200 F/g. The B-rG-O electrode had a low resistivity for ion movement, exhibited good stability after 4500 cycles, and showed a good rate response. These results illustrate the promise of B-rG-O systems for use as supercapacitor electrode materials.

METHOD

Preparation of B-rG-O. GO was synthesized from natural graphite (SP-1, Bay Carbon, MI) by the modified Hummers method as previously reported.[35] GO powder (500 mg) was loaded in a 250 mL round-bottom flask and purified water (167 mL) was added. A suspension (3 mg of GO/1 mL of water) was produced by sonication of GO powder with a Bransonic 8510 ultrasonic cleaner (250 W) until it became clear without visible GO particles. A solution of borane–THF adduct (1.5 mL, Sigma-Aldrich) was added to the suspension with stirring. The flask was then immersed in an oil bath, and the brown suspension was stirred under reflux with a magnetic stirring bar for 4 days. The resulting black solid product (B-rG-O) was filtered and dried under vacuum at room temperature for 12 h.

Measurements of Specific Capacitance. A two-electrode cell configuration was used to measure the performance of B-rG-O as a supercapacitor electrode in 6 M KOH solution. Polytetrafluoroethylene (PTFE, Sigma-Aldrich; 60 wt % dispersion in water) was added to the B-rG-O powder (B-rG-O/PTFE = 95:5 by weight) as a binder. The B-rG-O powder was mixed into a paste using a mortar and pestle, rolled into sheets of uniform thickness ranging from 40 to 50 μm thick (from sheet to sheet) and punched into 0.5 in. diameter electrodes after drying at 100 °C under vacuum. Two nearly identical (by weight and size) electrodes were assembled in a test cell consisting of two current collectors, two electrodes, and an ion-porous separator (Celgard 3501) supported in a test fixture consisting of two stainless steel plates. The mass of each electrode is between 1.5 and 2.5 mg.

For the three-electrode cell configuration, the slurry containing PTFE and B-rG-O (B-rG-O:PTFE = 95:5 by weight) was pressed onto a nickel form (1 cm × 1 cm) and dried at 100 °C under vacuum for use as the working electrode. The three-electrode cell consisted of a Pt sheet and saturated calomel electrode as the counter and reference electrodes, respectively.

Gravimetric capacitance for a single electrode was calculated from the discharge curve in a two-electrode cell as

$$C_{\text{single}} = \frac{4I\Delta t}{m\Delta V}$$

where I is the constant current and m is the total mass for both carbon electrodes, Δt is the discharge time, and ΔV is the voltage change during the discharge process.

Gravimetric capacitance in a three-electrode cell was obtained as

$$C_{\text{single}} = \frac{I\Delta t}{m_s\Delta V}$$

where I is the constant current and m_s is the mass of the working electrode, Δt is the discharge time and ΔV is the voltage change during the discharge process.

The surface area normalized capacitance C_{SA} (μF/g) was estimated from

$$C_{SA} = \frac{C_{\text{single}}}{S_{\text{BET}}} \times 100$$

where S_{BET} is the specific surface area (m^2/g) derived from the N_2 adsorption and C_{single} is the gravimetric capacitance in F/g.

Conflict of Interest: The authors declare no competing financial interest.

Acknowledgment. SP thanks Dr. Jong-Seong Bae in Korea Basic Science Institute (KBSI) for the XPS analysis. This work was supported by the Inha University. JH, SL, JO and SP were supported by Grants from the Center for Advanced Soft Electronics (Code No. 2011-0031629) under the Global Frontier Research Program of the Ministry of Education, Science and Technology, Korea and from the International Cooperation of the Korea Institute of Energy Technology Evaluation and Planning (KETEP) under the Ministry of Knowledge Economy, Korea. LLZ, JRP, and RSR appreciate funding support from the U.S. Department of Energy (DOE) under award DE-SC0001951.

Supporting Information Available: Experimental details, XPS, FT-IR, and Raman spectra, and powder conductivity and electrochemical measurement. This material is available free of charge *via* the Internet at http://pubs.acs.org.

REFERENCES AND NOTES

1. Dai, L.; Chang, D. W.; Baek, J.-B.; Lu, W. Carbon Nanomaterials for Advanced Energy Conversion and Storage. *Small* **2012**, *8*, 1130–1166.
2. Zhang, L. L.; Zhao, X. S. Carbon-Based Materials as Supercapacitor Electrodes. *Chem. Soc. Rev.* **2009**, *38*, 2520–2531.
3. Zhu, Y.; Murali, S.; Cai, W.; Li, X.; Suk, J. W.; Potts, J. R.; Ruoff, R. S. Graphene and Graphene Oxide: Synthesis, Properties, and Applications. *Adv. Mater.* **2010**, *22*, 3906–3924.
4. Chen, L.-F.; Zhang, X.-D.; Liang, H.-W.; Kong, M.; Guan, Q.-F.; Chen, P.; Wu, Z.-Y.; Yu, S.-H. Synthesis of Nitrogen-Doped Porous Carbon Nanofibers as an Efficient Electrode Material for Supercapacitors. *ACS Nano* **2012**, *6*, 7092–7102.
5. Park, S.; Ruoff, R. S. Chemical Methods for The Production of Graphenes. *Nat. Nanotechnol.* **2009**, *4*, 217–224.
6. Wang, G.; Zhang, L.; Zhang, J. A Review of Electrode Materials for Electrochemical Supercapacitors. *Chem. Soc. Rev.* **2012**, *41*, 797–828.
7. Kim, J. E.; Han, T. H.; Lee, S. H.; Kim, J. Y.; Ahn, C. W.; Yun, J. M.; Kim, S. O. Graphene Oxide Liquid Crystals. *Angew. Chem., Int. Ed.* **2011**, *50*, 3043–3047.
8. Yun, J. M.; Kim, K. N.; Kim, J. Y.; Shin, D. O.; Lee, W. J.; Lee, S. H.; Lieberman, M.; Kim, S. O. DNA Origami Nanopatterning on Chemically Modified Graphene. *Angew. Chem.* **2012**, *124*, 936–939.
9. Hwang, J. O.; Park, J. S.; Choi, D. S.; Kim, J. Y.; Lee, S. H.; Lee, K. E.; Kim, Y.-H.; Song, M. H.; Yoo, S.; Kim, S. O. Workfunction-Tunable, N-doped Reduced Graphene Transparent Electrodes for High-Performance Polymer Light-Emitting Diodes. *ACS Nano* **2012**, *6*, 159–167.
10. Panchakarla, L. S.; Subrahmanyam, K. S.; Saha, S. K.; Govindaraj, A.; Krishnamurthy, H. R.; Waghmare, U. V.; Rao, C. N. R. Synthesis, Structure, and Properties of Boron- and Nitrogen-Doped graphene. *Adv. Mater.* **2009**, *21*, 4726–4730.

11. Martins, T. B.; Miwa, R. H.; da Silva, A. J. R.; Fazzio, A. Electronic and Transport Properties of Boron-Doped Graphene Nanoribbons. *Phys. Rev. Lett.* **2007**, *98*, 196803.
12. Wu, Z.-S.; Ren, W.; Xu, L.; Li, F.; Cheng, H.-M. Doped Graphene Sheets as Anode Materials with Super High Rate and Large Capacity for Lithium Ion Batteries. *ACS Nano* **2011**, *7*, 5463–5471.
13. Lu, X.; Wu, J.; Lin, T.; Wan, D.; Huang, F.; Xie, X.; Jiang, M. Low-Temperature Rapid Synthesis of High-Quality Pristine or Boron-Doped Graphene *via* Wurtz-Type Reductive Coupling Reaction. *J. Mater. Chem.* **2011**, *21*, 10685–10689.
14. Zhang, L. L.; Zhou, R.; Zhao, X. S. Graphene-Based Materials as Supercapacitor Electrodes. *J. Mater. Chem.* **2010**, *20*, 5983–5992.
15. Stoller, M. D.; Park, S.; Yanwu, Z.; An, J.; Ruoff, R. S. Graphene-Based Ultracapacitors. *Nano Lett.* **2008**, *8*, 3498–3502.
16. Zhu, Y.; Murali, S.; Stoller, M. D.; Ganesh, K. J.; Cai, W.; Ferreira, P. J.; Pirkle, A.; Wallace, R. M.; Cychosz, K. A.; Thommes, M.; *et al*. Carbon-Based Supercapacitors Produced by Activation of Graphene. *Science* **2011**, *332*, 1537–1541.
17. Xu, B.; Yue, S.; Sui, Z.; Zhang, X.; Hou, S.; Cao, G.; Yang, Y. What Is the Choice for Supercapacitors: Graphene or Graphene Oxide? *Energy Environ. Sci.* **2011**, *4*, 2826–2830.
18. Brownson, D. A. C.; Banks, C. E. Fabricating Graphene Supercapacitors: Highlighting the Impact of Surfactants and Moieties. *Chem. Commun.* **2012**, *48*, 1425–1427.
19. Lin, Z.; Liu, Y.; Yao, Y.; Hildreth, O. J.; Li, Z.; Moon, K.; Wong, C.-P. Superior Capacitance of Functionalized Graphene. *J. Phys. Chem. C* **2011**, *115*, 7120.
20. Chen, Y.; Zhang, X.; Zhang, D.; Yu, P.; Ma, Y. High Performance Supercapacitors Based on Reduced Graphene Oxide in Aqueous and Ionic Liquid Electrolytes. *Carbon* **2011**, *49*, 573–580.
21. Park, S.; Hu, Y.; Hwang, J. O.; Lee, E.-S.; Casabianca, L. B.; Cai, W.; Potts, J. R.; Ha, H.-W.; Chen, S.; Oh, J.; *et al*. Chemical Structures of Hydrazine-Treated Graphene Oxide and Generation of Aromatic Nitrogen Doping. *Nat. Commun.* **2012**, *3*, 638.
22. Conway, B. E. *Electrochemical Supercapacitors: Scientific Fundamentals and Technological Applications*; Kluwer Academic/Plenum Publisher: New York, 1999.
23. Cao, X.; Shi, Y.; Shi, W.; Lu, G.; Huang, X.; Yan, Q.; Zhang, Q.; Zhang, H. Preparation of Novel 3D Graphene Networks for Supercapacitor Applications. *Small* **2011**, *7*, 3163–3168.
24. Liu, C.; Yu, Z.; Neff, D.; Zhamu, A.; Jang, B. Z. Graphene-Based Supercapacitor with an Ultrahigh Energy Density. *Nano Lett.* **2010**, *10*, 4863–4868.
25. Yu, G.; Hu, L.; Vosgueritchian, M.; Wang, H.; Xie, X.; McDonough, J. R.; Cui, X.; Cui, Y.; Bao, Z. Solution-Processed Graphene/MnO_2 Nanostructured Textiles for High-Performance Electrochemical Capacitors. *Nano Lett.* **2011**, *11*, 2905–2911.
26. Wu, Z.-S.; Ren, W.; Wang, D.-W.; Li, F.; Liu, B.; Cheng, H.-M. High-Energy MnO_2 Nanowire/Graphene and Graphene Asymmetric Electrochemical Capacitors. *ACS Nano* **2010**, *4*, 5835–5842.
27. Fan, Z.; Yan, J.; Wei, T.; Zhi, L.; Ning, G.; Li, T.; Wei, F. Asymmetric Supercapacitors Based on Graphene/MnO_2 and Activated Carbon Nanofiber Electrodes with High Power and Energy Density. *Adv. Funct. Mater.* **2011**, *21*, 2366–2375.
28. Mishra, A. K.; Ramaprabhu, S. Functionalized Graphene-Based Nanocomposites for Supercapacitor Application. *J. Phys. Chem. C* **2011**, *115*, 14006–14013.
29. Kumar, N. A.; Choi, H.-J.; Shin, Y. R.; Chang, D. W.; Dai, L.; Baek, J.-B. Polyaniline-Grafted Reduced Graphene Oxide for Efficient Electrochemical Supercapacitors. *ACS Nano* **2012**, *6*, 1715–1723.
30. Stoller, M. D.; Magnuson, C. W.; Zhu, Y.; Murali, S.; Suk, J. W.; Piner, R.; Ruoff, R. S. Interfacial Capacitance of Single Layer Graphene. *Energy Environ. Sci.* **2011**, *4*, 4685–4689.
31. Wang, D.-W.; Li, F.; Chen, Z.-G.; Lu, G. Q.; Cheng, H.-M. Synthesis and Electrochemical Property of Boron-Doped Mesoporous Carbon in Supercapacitor. *Chem. Mater.* **2008**, *20*, 7195–7200.
32. Guo, H.; Gao, Q. Boron and Nitrogen Co-Doped Porous Carbon and Its Enhanced Properties as Supercapacitor. *J. Power Sources* **2009**, *186*, 551–556.
33. Kwon, T.; Nishihara, H.; Itoi, H.; Yang, Q., -H.; Kyotani, T. Enhancement Mechanism of Electrochemical Capacitance in Nitrogen-/Boron-Doped Carbons with Uniform Straight Nanochannels. *Langmuir* **2009**, *25*, 11961–11968.
34. Dreyer, D. R.; Park, S.; Bielawski, C. W.; Ruoff, R. S. The Chemistry of Graphene Oxide. *Chem. Soc. Rev.* **2010**, *39*, 228–240.
35. Park, S.; An, J.; Piner, R. D.; Jung, I.; Yang, D.; Velamakanni, A.; Nguyen, S. T.; Ruoff, R. S. Aqueous Suspension and Characterization of Chemically Modified Graphene Sheets. *Chem. Mater.* **2008**, *20*, 6592–6594.
36. He, H.; Klinowski, J.; Forster, M.; Lerf, A. New A Structural Model for Graphite Oxide. *Chem. Phys. Lett.* **1998**, *287*, 53–56.
37. Cai, W.; Piner, R. D.; Stadermann, F. J.; Park, S.; Shaibat, M. A.; Ishii, Y.; Yang, D.; Velamakanni, A.; An, S. J.; Stoller, M.; *et al*. Synthesis and Solid-State NMR Structural Characterization of ^{13}C-Labeled Graphite Oxide. *Science* **2008**, *321*, 1815–1817.
38. Staubitz, A.; Robertson, A. P. M.; Sloan, M. E.; Manners, I. Amine- and Phosphine-Borane Adducts: New Interest in Old Molecules. *Chem. Rev.* **2010**, *110*, 4023–4078.
39. Wang, J.; Chen, Y.; Zhang, Y.; Ionescu, M. I.; Li, R.; Sun, X.; Ye, S.; Knights, S. 3D Boron Doped Carbon Nanorods/Carbon-Microfiber Hybrid Composites: Synthesis and Applications in a Highly Stable Proton Exchange Membrane Fuel Cell. *J. Mater. Chem.* **2011**, *21*, 18195–18198.
40. Jacobsohn, L. G.; Schulze, R. K.; da Costa, M. E. H. M.; Nastasi, M. X-ray Photoelectron Spectroscopy Investigation of Boron Carbide Films Deposited by Sputtering. *Surf. Sci.* **2004**, *572*, 418–424.
41. Park, S.; Lee, K.-S.; Bozoklu, G.; Cai, W.; Nguyen, S. T.; Ruoff, R. S. Graphene Oxide Papers Modified by Divalent Ions—Enhancing Mechanical Properties *via* Chemical Cross-Linking. *ACS Nano* **2008**, *2*, 572–578.
42. Yang, D.; Velamakanni, A.; Bozoklu, G.; Park, S.; Stoller, M.; Piner, R. D.; Stankovich, S.; Jung, I.; Field, D. A.; Ventrice, J. C. A.; *et al*. Chemical Analysis of Graphene Oxide Films after Heat and Chemical Treatments by X-ray Photoelectron and Micro-Raman Spectroscopy. *Carbon* **2009**, *47*, 145–152.
43. Barton, D. H. R.; Jacob, M. Phosphine-Boranes as Selective Reagents for the Radical Deoxygenation of a Hindered Secondary Alcohol. *Tetrahedron Lett.* **1998**, *39*, 1331–1334.
44. Lau, C. K.; Tardif, S.; Dufresne, C.; Scheigetz, J. Reductive Deoxygenation of Aryl Aldehydes and Ketones by *tert*-Butylamine−Borane and Aluminum Chloride. *J. Org. Chem.* **1989**, *54*, 491–494.
45. Kim, D.-H.; Ryu, E.-S.; Cho, C. S.; Shim, S. C.; Kim, H.-S.; Kim, T.-J. Reductive Deoxygenation of a-Ferrocenyl Carbonyls and Alcohols to Alkylferrocenes by Borane-Dimethyl Sulfide. *Organometallics* **2000**, *19*, 5784–5786.
46. Park, S.; An, J.; Jung, I.; Piner, R. D.; An, S. J.; Li, X.; Velamakanni, A.; Ruoff, R. S. Colloidal Suspensions of Highly Reduced Graphene Oxide in a Wide Variety of Organic Solvents. *Nano Lett.* **2009**, *9*, 1593–1597.
47. Nakamoto, K. *Infrared and Raman Spectra of Inorganic and Coordination Compounds*, 4th ed.; John Wiley & Sons: New York, 1986.
48. Stankovich, S.; Dikin, D. A.; Piner, R.; Kohlhaas, K. M.; Kleinhammes, A.; Jia, Y.; Wu, Y.; Nguyen, S. T.; Ruoff, R. S. Synthesis of Graphene-Based Nanosheets *via* Chemical Reduction of Exfoliated Graphite Oxide. *Carbon* **2007**, *45*, 1558–1565.
49. Zhao, L.; Fan, L.-Z.; Zhou, M.-Q.; Guan, H.; Qiao, S.; Antonietti, M.; Titirici, M.-M. Nitrogen-Containing Hydrothermal Carbons with Superior Performance in Supercapacitors. *Adv. Mater.* **2010**, *22*, 5202–5206.
50. Guo, H.; Gao, Q. Boron and Nitrogen Co-Doped Porous Carbon and Its Enhanced Properties as Supercapacitor. *J. Power Sources* **2009**, *186*, 551–556.

51. Zhang, L. L.; Zhao, X.; Ji, H.; Stoller, M. D.; Lai, L.; Murali, S.; McDonnell, S.; Cleveger, B.; Wallace, R. M.; Ruoff, R. S. Nitrogen Doping of Graphene and Its Effect on Quantum Capacitance, and a New Insight on the Enhanced Capacitance of N-Doped Carbon. *Energy. Environ. Sci.* **2012**, *5*, 9618–9625.
52. Gao, W.; Alemany, L. B.; Ci, L.; Ajayan, P. M. New Insights into the Structure and Reduction of Graphite Oxide. *Nat. Chem.* **2009**, *1*, 403–408.
53. Si, Y.; Samulski, E. T. Synthesis of Water Soluble Graphene. *Nano Lett.* **2008**, *8*, 1679–1682.